# Morphology of Ultrathin Supported Diblock Copolymer Films: Theory and Experiment

**Michael J. Fasolka,[†] Pallab Banerjee, and Anne M. Mayes***

*Department of Materials Science and Engineering, Massachusetts Institute of Technology, Cambridge, Massachusetts 02139*

**Galen Pickett[‡] and Anna C. Balazs**

*Department of Chemical and Petroleum Engineering, University of Pittsburgh, Pittsburgh, Pennsylvania 15620*

*Received January 8, 1999; Revised Manuscript Received March 6, 2000*

ABSTRACT: An analysis of the morphological behavior of substrate-supported diblock copolymer films for thicknesses $t$ below the equilibrium period $L_0$ of the copolymer is presented. Substrate-supported films generally exhibit dissimilar interactions between the copolymer block components and the free and substrate surfaces. Accordingly, in this study, self-consistent-field calculations that incorporate asymmetric surface energetics were used to assess equilibrium film morphologies. Phase diagrams were constructed as a function of film thickness, surface interaction energies, the segmental interaction, and the chain length. In conjunction, experiments were conducted on a series of polystyrene-*b*-poly(*n*-alkyl methacrylate) copolymer films supported by silicon substrates. These employed a novel atomic force microscopy technique that allowed for the precise tracking of morphology as a function of film thickness. Comparison of the experimental results and calculations revealed several common trends. In particular, hybrid morphologies, incorporating both surface-parallel and surface-perpendicular elements, were observed both experimentally and through the calculations for the thickness regime, $t \sim 0.5L_0$. The stability of such structures was found to be closely linked to the symmetry of the surface energetics.

## Introduction

Diblock copolymers microphase separate to form patterns of regularly sized domains spaced at an equilibrium period, $L_0$, characteristic of the chain length, the segmental interaction, and the relative volume fraction of the block components.[1] In bulk systems, microphase separation is typified by grains of certain inclination oriented randomly with respect to each other. Each of these features—strong adherence to an equilibrium period and lack of common orientation—is characteristic of systems that lack strong surface boundary conditions.

Dominating the behavior of diblock copolymer (hereafter, DBC) thin films are effects imposed by surface boundary conditions. Indeed, the unique morphological trends these systems display denote an interplay between surface/interfacial interactions and the natural and spontaneous ordering activity of the bulk material. A simple example of this is illustrated by considering a film of compositionally symmetric DBC (which exhibits a lamellar morphology in bulk) supported by a substrate. Typically, films of thickness $t > L_0$ form lamellae oriented perfectly parallel with the substrate surface (Figure 1A). This morphology satisfies the substrate boundary condition, which demands contact with the block having more favorable substrate interactions. The free surface presents a similar boundary condition which favors the expression of the lower surface energy ($\gamma$) block at this interface. Substrate-parallel lamellae constitute a morphology that conforms to these demands, minimizes the block–block interfacial area, and preserves the natural periodicity of the material. Several published works, both experimental[2–7] and theoretical,[8–12] have explored the basics and intricacies of this well-understood thin film system.

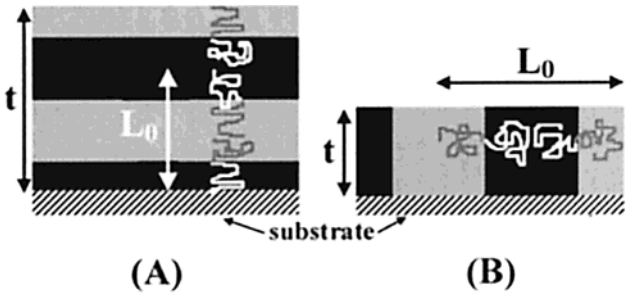


**Figure 1.** Schematic cross sections of DBC thin film morphologies: (A) surface-parallel lamellae, typical of films with thickness $t$ greater than the equilibrium period, $L_0$; (B) surface-perpendicular lamellae are often formed when the film thickness is less than $L_0$.

More complicated behavior is exhibited by DBC thin film systems for films of thickness $t < L_0$. In this case, the formation of a surface-parallel lamellar phase would incur an entropic penalty, since the chains would be forced into "compressed" microphase domains. Accordingly, such constrained systems sometimes adopt a morphology where lamellae are oriented perpendicular to the film surface plane (Figure 1B).[13–16] This arrangement maximizes the conformational entropy of the chains by allowing $L_0$ to be expressed laterally. Such lateral morphologies are particularly interesting because they offer the possibility of designing nanometer scale chemically patterned surfaces.[17–21]

The above observation illustrates the *thickness dependence* of DBC thin film morphology. Thickness trends in domain orientation were first predicted by

[†] Current address: Optical Technology Division, N.I.S.T., Gaithersburg, MD 20899.

[‡] Current address: Department of Physics, University of Illinois, Champagne–Urbana, IL 61801.

10.1021/ma990021h CCC: $19.00 
Published on Web 00/00/0000 PAGE EST: 10.3

Walton et al.[14] and Kikuchi and Binder.[12] More recent studies have been completed by Matsen,[22] Pickett and Balazs,[23] and Tang and Witten,[24] among others.[25−27] Experimental observations have been published by several groups who have explored the thickness dependence of film morphology in free-standing,[28] sandwiched,[16,29−31] and substrate-supported films.[6,7,13,15,19,20,32−38] In total, these studies reveal the following trends. First, DBC domain orientation (or even domain motif!)[39] changes as a function of film thickness. In particular, substrate perpendicular domain orientations occur when the film thickness is not commensurate with the equilibrium period of the ordered copolymer. This is especially true when $t < L_0$ or if the film is confined between hard walls. Second, surface boundary energetics greatly affect the domain orientation, as demonstrated by Kellogg et al.[16] for films sandwiched between identical attractive surfaces and Lambooy et al.[29] and Huang et al.[20,35] for diblock films between surfaces that are chemically neutral with respect to the two blocks.

In large part, the theoretical treatments of thin film diblock morphologies noted above have examined the case where surface boundary conditions are symmetric.[9,12,14,22,23,25−27] In such treatments, the interactions between a given monomer type and each surface are modeled as either neutral or equal in magnitude. While this approach well captures the physics of free-standing films and films sandwiched between chemically identical surfaces, it less adequately describes the case of substrate supported films, which are generally characterized by highly *asymmetric boundary conditions*. Indeed, as discussed below, in supported film systems the monomer−surface interaction can differ from the monomer−substrate interaction by an order of magnitude. The need to address such asymmetric boundary conditions is made evident by the fact that, in many cases, supported films tend to be more tractable from an experimental standpoint given the inherent delicacy of ultrathin systems. Moreover, such supported diblock film systems are recognized as promising candidates for nanoscale device technologies.[17−19,21,40] Walton and coworkers[14] and Matson[22] have each considered the case of asymmetric boundary conditions on thin diblock films. However, these previous treatments mainly examine thicknesses above $L_0$. Further, these studies made a priori assumptions regarding the equilibrium film structure that did not include the possibility of combination surface-parallel/surface-perpendicular morphologies for thicknesses near to or beneath $L_0$. Experimental evidence of these "hybrid" structures is documented in previous studies[19,33] and in the current work.

With this motivation, theoretical and experimental techniques were developed to study the thickness-dependent morphology of DBC thin films with asymmetric boundary conditions when $t \leq L_0$. The following pages describe this work, first through a discussion of self-consistent-field (SCF) calculations designed to model substrate-supported DBC thin films. This will be followed by an explication of a series of experiments, conducted on thin films of a family of polystyrene-*b*-poly(*n*-alkyl methacrylate) copolymers supported by silicon substrates. These measurements employed atomic force microscopy (AFM) in such a way as to pinpoint the exact film thicknesses at which morphological transitions occur. Correlations and differences between the SCF calculations and the AFM measurements will be discussed.

## Methodology: Self-Consistent-Field Calculations

Two-dimensional self-consistent field calculations were performed following the approach of Scheutjens and Fleer,[41] recently applied to the case of DBC thin films by Pickett and Balazs.[23] Compositionally symmetric DBCs (equal block volumes) were modeled on a lattice as chains $N$ statistical segments in length, each segment occupying one lattice space, with $N/2$ contiguous segments of type A and the remaining of type B. Thin films were modeled by confining chains to a rectangular lattice $t$ units high ($x$) and $r > t$ units long ($y$). The lattice length, $r$, was chosen to be as large as permissible computationally (30−40 lattice units) and such that it did not coincide with any multiples or half-multiples of the copolymer periodicity, $L_0$. The $x = 0$ and $x = t$ boundaries were impenetrable while the $y = 0$ and $y = r$ boundaries were taken as reflecting. The impenetrable "film surface" boundaries (hereafter $S_1$ at $x = 0$ and $S_2$ at $x = t$) were energetically selective of the B monomers. This was accomplished through variable attractive interactions between B segments and each of these surfaces, denoted $S_1^B$ and $S_2^B$, and equal in magnitude but opposite in sign repulsive interactions with the A segments, i.e., $S_1^A = -S_1^B$ and $S_2^A = -S_2^B$.[42] Several sets of calculations were completed for which $S_1^B$ values were held at −0.1, −0.2, −0.3, −0.5, −0.7, and −0.9 $kT$. For each of these calculation sets, $S_2^B$ interactions varied between 0 $kT$ and $S_1^B$ for that set (i.e., $0\ kT \leq S_2^B \leq S_1^B$). These asymmetric interactions model a supported film system in which the B monomers are favored to reside at both the substrate *and* the free surface, but for which the substrate interaction is much stronger. In addition, for one system, *antisymmetric* interactions were imposed. For this set of calculations, discussed toward the end of this paper, $S_1^B$ was −0.3 $kT$, while $S_2^B$ varied from 0 to $-S_1^B$, with $S_1^A = -S_1^B$ and $S_2^A = -S_2^B$. In this case, the $S_1$ surface attracts B segments while the $S_2$ surface prefers A segments, but with a differing magnitude of attraction.

SCF calculations hinge upon the interdependence of the potential field, $U(x,y)$, and the statistical segment density field, $f(x,y)$, in the model system. The probability that a specific segment occupies a given lattice site depends on the various segment−segment and surface potentials surrounding that site. Likewise, the spatial distribution of the segmental potentials depends on how segments are apportioned in the system. Following Scheutjens and Fleer,[41] $f(x,y)$ and $U(x,y)$ are iteratively calculated until a self-consistent solution, in which $f(x,y)$ directly implies $U(x,y)$ at each $(x,y)$, is found. In our calculations, this iterative process also included the constraint that the total density function $f_T = f_A + f_B = 1.0$ at all $(x,y)$, meaning the system was incompressible. Additionally, the calculated solution was directed to arrive, at least locally, at a free energy minimum. While it is difficult to demonstrate definitively that any calculated morphology represents the global free energy minimum, multiple sets of initial conditions were employed, with the purpose of increasing the range of morphologies calculated and thus the probability of finding the true equilibrium. It may be noted here that these SCF calculations make *no* a priori assumptions as to the shape of the A/B interface, as in the case of previous theoretical treatments of similar systems.[22] While this makes the compilation of free energy data

**Table 1. $L_0$ Values from SCF Calculations (in Units of Lattice Spacing)**

| $N$ | $\chi_{AB} = 0.1$ | $\chi_{AB} = 0.15$ | $\chi_{AB} = 0.2$ |
|---|---|---|---|
| 100 | 14 | | |
| 125 | 16 | | |
| 150 | 19 | 21 | 23 |
| 200 | 24 | 26 | 28 |
| 250 | 28 | | |

for the purposes of generating phase diagrams more difficult (see below), it opens the possibility of finding novel morphologies, as our results will show.

Four copolymer lengths, $N$, and three segmental interaction parameters ($\chi_{AB}$) were used in the calculations. The equilibrium periods, $L_0$, of molecules with given $N$ and $\chi_{AB}$ were determined by calculating the free energy ($F$) of surface-parallel lamella existing between two reflecting boundaries while varying the system thickness, $t$. The $t$ that gave the lowest $F$ was taken as $L_0$ for the molecule. Table 1 gives the $L_0$ values calculated for the copolymer chains studied.

For each molecule in Table 1, $t$ was decreased from $L_0$ to $L_0/4$ in single lattice unit steps. For each film thickness, the regimen of surface energetics described above was applied. The generation of phase diagrams from the calculations requires that free energy values for a variety of morphologies be calculated for each set of surface energies and each film thickness. In this study, the free energy space of the system was sufficiently mapped out using the following techniques. First, by employing various initial conditions, the calculations could be directed to a variety of energetic minima representing different morphologies. Additionally, it was found that for constant $t$ the free energy curves for surface-parallel morphologies (full and half lamella, discussed below) were *linear* functions of the ratio of the surface interactions ($S_2^B/S_1^B$). This trend was previously predicted from the analytical model of Walton et al.[14] Using this fact, $F$ for these morphologies could be accurately estimated for cases in which the SCF calculations did not produce them. This extrapolation of $F$ data was tested against cases in which the data were actually calculated, showing that such estimates were true to within 3%.

Phase diagrams were produced through an analysis of the free energy data. The free energy spaces (as a function of $t$ and $S_2^B/S_1^B$) were compiled for each of the morphologies predicted by the calculations. Phase boundaries between two given morphologies were found by calculating their free energy difference as a function of $t$ and estimating the thickness at which this difference vanished via a linear interpolation.

## Materials and Methodology: Experiment

Table 2 lists the polystyrene-*b*-poly(*n*-alkyl methacrylate) block copolymers employed in the experimental portion of this study. Included in this table are the abbreviated names by which the copolymers will be referred. The synthesis and characterization of these materials are described elsewhere.[43] These copolymers have the following common traits. First, they are approximately symmetric by volume and thus produce a lamellar morphology in bulk as verified by transmission electron microscopy (TEM) on ultra-microtomed bulk samples. Second, with the exception of polystyrene-*b*-poly(methyl methacrylate) (PS-*b*-PMMA), for thin films on silicon, the methacrylate block is favored to reside at both the free surface and adjacent to the silicon substrate.[44] The favorable substrate interaction is due to hydrogen bonding between the methacrylate carbonyl groups and hydroxyl groups terminating the passive oxide layer known to form on silicon. At the free surface the methacrylates (with the exception of PMMA) are favored because they have a lower surface energy than polystyrene. The last column in Table 1 shows a rough estimate of the ratio of the free and substrate surface interactions ($E_{FS}$ and $E_{sub}$, respectively) calculated as

$$E_{FS}/E_{sub} = (\gamma^{PS} - \gamma^{PnMA})/(E_{HB}/S_M) \quad (1)$$

where $\gamma^{PS} - \gamma^{PnMA}$ is the difference in surface tension between polystyrene and the particular poly(*n*-alkyl methacrylate), $E_{HB}$ is the strength of the hydrogen bond (conservatively estimated as 4 kcal/mol[45] or 4.8 $kT$), and $S_M$ is the surface area (per mole) of the methacrylate monomer expressed at the substrate, calculated from the molar volume of the methacrylate monomer as $S_M = (V_M/N_{AV})^{2/3}N_{AV}$, where $V_M$ is the molar volume and $N_{AV}$ is Avogadro's number. While only an approximation, this table of values reveals the asymmetry of the surface boundary energetics in the experimental thin film systems; in each case, the ratio indicates about an order of magnitude increase in substrate interaction as compared to the case of the free surface. Note that the degree of asymmetry increases with decreasing side chain length, while for PS-*b*-PMMA, $E_{FS}/E_{sub}$ is negative, due to the higher surface energy of PMMA as compared to that of PS. This system exhibits, for $t > L_0$, a surface-parallel lamellar structure which has PMMA at the silicon substrate and PS at the free surface.[3] Also included in Table 1 are $\chi_{AB}$ values measured for these diblock systems[43,46,47] and statistical segment lengths, $a$, for the methacrylate blocks.

Substrates were polished silicon wafers (RMS roughness ~5 Å) with a native oxide surface. Wafers were precleaned via ultrasonication for 1 h in toluene followed by a 24 h immersion in chromic−sulfuric acid, 5 min rinsing under deionized water, and air-drying. DBC films were solution cast onto these substrates from toluene, a common solvent to PS and the *n*-alkyl methacrylates. For TEM work, solutions were spin-cast from a 0.5% w/v concentration at 1000 rpm, resulting in 20−70 nm thick films as determined by ellipsometry. For AFM analysis, droplets of 0.1% w/v solution were deposited onto the substrates via a micropipet. The toluene was allowed to evaporate in air, leaving a fine ring of copolymer "microdroplets" deposited by the receding solvent.[7] These microdroplets exhibit a *profile of film thickness* (from 0 at the edges to about 200 nm at the apex) which allows us to chart the thickness dependence of copolymer morphology in a precise manner via AFM. Annealing (at least 72 h at 180 °C) induces directed ordering in the films and droplets. Ordered microdroplets

**Table 2. Polystyrene-*b*-poly(*n*-alkyl methacrylate) Diblock Copolymers Used in Experimental Analysis**

| block copolymer | methacrylate block component | mol wt, $M_n$ (g/mol) | $L_0$ (nm) | $\chi_{AB}$ ($kT$) | statistical segment length, $a$ (nm) | $E_{FS}/E_{sub}$ |
|---|---|---|---|---|---|---|
| PS-*b*-PLMA 170 | lauryl methacrylate | 170K | 54.4 ± 1.1 | 0.085[43] | 1.5[43] | 0.17 |
| PS-*b*-PLMA 50 | lauryl methacrylate | 50K | 23.6 ± 0.4 | 0.085 | 1.5 | 0.17 |
| PS-*b*-PHMA | hexyl methacrylate | 70K | 37.4 ± 0.8 | 0.044[43] | 1.08[43] | 0.165 |
| PS-*b*-PBMA 140 | butyl methacrylate | 140K | 43.1 ± 0.8 | 0.015[47] | 0.86[47] | 0.13 |
| PS-*b*-PBMA 250 | butyl methacrylate | 250K | 61.5 ± 0.9 | 0.015 | 0.86 | 0.13 |
| PS-*b*-PBMA 650 | butyl methacrylate | 650K | 121 ± 2 | 0.015 | 0.86 | 0.13 |
| PS-*b*-PPMA | propyl methacrylate | 120K | 47.9 ± 0.7 | 0.01[47] | 0.84[47] | 0.09 |
| PS-*b*-PEMA | ethyl methacrylate | 120K | 49.4 ± 1 | 0.013[47] | 0.83[47] | 0.05 |
| PS-*b*-PMMA | methyl methacrylate | 125K | 51.0 ± 1.0 | 0.038[46] | 0.64[65] | −0.004 |

exhibit a stepped profile indicative of discrete layers of surface-parallel lamellae—each "step" being $L_0$ high.[5,7,13,48] This ordering is made evident under optical microscopy as sharp bands of color caused by specific film thickness−interference conditions.

**TEM.** Spin-cast samples were prepared for TEM by peeling the films from their substrates. Here, we adapt a method first used to create carbon replicas of surface features for examination with TEM.[49,50] The films were coated with a thermally evaporated 10 nm layer of carbon. Next, a macroscopic (∼1 mm) layer of aqueous poly(acrylic acid) solution (25% w/v) was poured over the samples. Upon drying, this poly(acrylic acid) (PAA) layer contracts, pulling the sample and carbon support layer, intact, from the substrate.[19,51] Next, the sample is carefully placed (PAA side down) on a pool of deionized water. The PAA layer dissolves, leaving a floating sample that can be retrieved with a copper TEM grid. Some of these retrieved samples were embedded in epoxy and ultramicrotomed for cross-sectional analysis. All films were stained with $RuO_4$ for 10 min to preferentially stain the PS block. In the TEM images that follow, PS regions appear dark. Electron microscopy was accomplished via low-dose techniques on a JEOL 200CX using 200 kV electrons.

**AFM.** Microdroplet films were studied directly on their substrates with a Digital Instruments Dimension 3000 Multimode AFM in "tapping mode". Examined areas were designed to include both the droplet edge and some adjacent bare substrate. In this scheme, the bare substrate serves as a baseline against which topographic information on the droplet edge can be compared, providing an accurate and local measure of *film thickness.* Height measurements were completed in conjunction with simultaneous phase measurements. Phase data illuminate local elasticity variations by measuring the phase shift between the oscillation the AFM probe is being driven at and its vibration in the presence of the sample surface. In the images that follow, harder regions appear lighter as compared to softer domains. To optimize the elasticity contrast in the AFM phase images, the free-air probe oscillation amplitude ($A_0$) was maintained at 3 V while the surface-contact oscillation amplitude ($A_{sp}$) was 1.5 V, giving the established optimal ratio, $A_{sp}/A_0$, of 0.5.[52−54] The standard silicon nitride probes were driven just below the peak of their natural frequencies in the 300 kHz range. Contact forces were in the range of 15 nN.

This simultaneous measurement of phase and height data on microdroplet edges allows determination of the exact film thicknesses at which morphological transitions occur. Surface-parallel morphologies, which express only one block component at the free surface, are seen as featureless areas in the phase data scans. In contrast, surface-perpendicular morphologies exhibit a pattern of elasticity contrast in the phase images. In each case, the type of morphology can be correlated with film thickness data derived from the height image.

Morphology/thickness data were collected as follows. For each copolymer system, the lamellar period, $L_0$, was determined by measuring the height of steps on the ordered microdroplets. The film thicknesses at which morphological transitions occurred were determined by measuring the height difference between the substrate and points where phase contrast was first observed. All $L_0$ and transition thickness values were derived from 20 independent measurements across a given film. To minimize the effect of probe depression of the sample surface, transition thickness data are expressed relative to the $L_0$ measurements collected under identical tip tuning conditions. Typical tip depression of the sample surface is about 1 nm for polymers under these scan conditions.

## Results and Discussion

**SCF Calculations.** Figure 2a gives a summary of the four morphologies found with the SCF calculations presented in the order (with decreasing film thickness) in which they occur. The images shown are cross-sectional views of the film where $S_1$ is the top boundary and $S_2$ is the bottom boundary. The gradients depict the calculated density of B segments. Black indicates 100% B segments and white 100% A segments. Included below each image is the abbreviation used herein to identify that morphology. These morphologies can be separated into two categories, discussed below.

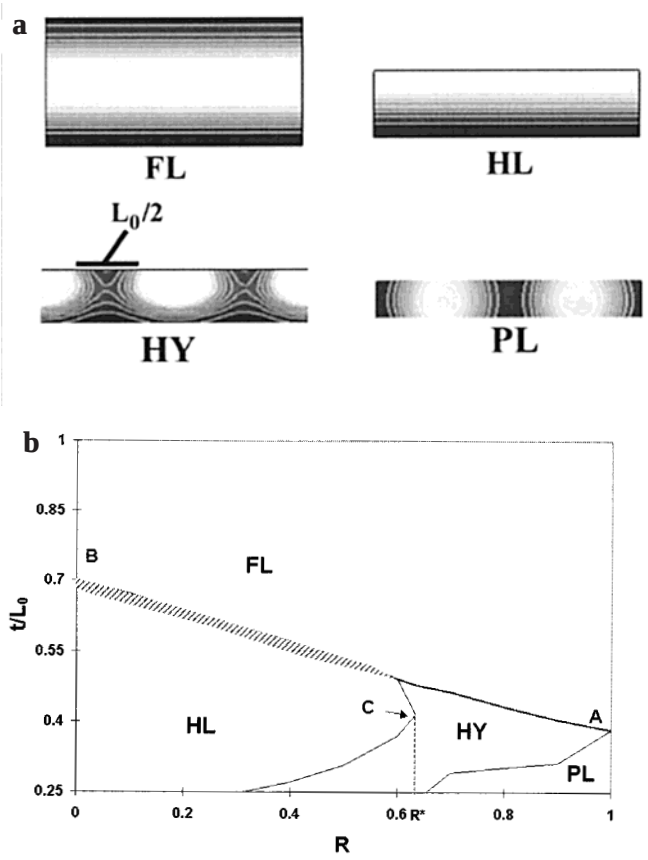


**Figure 2.** (a) Summary of morphologies illuminated by the SCF calculations. The morphologies are shown in cross section with the abbreviations by which they are referred to in the text. Black indicates 100% B segments and white 100% A. (b) Example phase diagram. $R = S_2^B/S_1^B$. $S_1^B = -0.3\ kT$, $N = 200$, and $\chi_{AB} = 0.1$. Phase fields are labeled with abbreviations found in (a). The gray area marks where the HY structure is metastable.

**1. Surface-Parallel Morphologies**. When $t \approx L_0$, the full surface-parallel lamellar morphology (FL) is seen, consisting of a domain of A sandwiched by layers of B blocks at each surface $S_1$ and $S_2$. This structure minimizes the surface and interfacial energetics while maintaining the natural period of the ordered state. When $t \approx 0.5L_0$, a surface-parallel half-lamellar (HL) morphology may be favorable. Here, the strong $S_1^B$ interaction forces the B block to $S_1$, while the A block resides at $S_2$. While this does not embody the most favorable surface energetics (B at *both* $S_1$ and $S_2$), the single flat A−B interface affords the minimum unfavorable contact between these immiscible blocks. Additionally, this structure preserves bulk period dimensions.

**2. Surface-Perpendicular Morphologies**. Two types of surface-perpendicular morphologies were noted. The first, which we term a "hybrid structure" (HY), seen in Figure 2a, consists of a layer of B at the $S_1$ surface with surface-perpendicular protrusions extending to the $S_2$ surface, perforating a layer of A. These perpendicular features are approximately $0.5L_0$ wide; i.e., they retain bulk period dimensions. The HY morphology resembles

the mixed-orientation lamellar phases predicted by Kikuchi and Binder[12] and other later studies.[22,24] However, in this previous work *noncontiguous* surface-parallel and surface-perpendicular domains were found for structures that occur near $t = L_0$,[12,24] or these mixed morphologies were found to be unstable.[22] In the current work, a stable HY structure is predicted to occur at thicknesses well below $L_0$, with *contiguous* surface-parallel and surface-perpendicular regions.

The second surface-perpendicular morphology, "perpendicular lamellae" (PL), consist of full lamellae arranged laterally with respect to the film surfaces. This morphology has been noted several times in previous theoretical studies.[14,22,23] Close inspection of the computed PL structure in Figure 2d shows that the A/B interfaces are not flat but are concave with respect to the B-segment domains. This curvature is consistent with earlier calculations modeling lamellae at a preferential wall by Pickett[55] and later by Pereira.[56]

For both perpendicular morphologies, the equilibrium spacing of the B-domains was determined as the lateral lattice dimension ($y$) that minimizes the free energy (per chain) of the system. Both the HY and PL morphologies exhibit an equilibrium lateral spacing equal to $L_0$.

Figure 2b shows an example phase diagram constructed from the SCF data. In this figure, $N = 200$, $\chi_{AB} = 0.1$, and $S_1^B = -0.3\ kT$. The ordinate is reduced film thickness ($t/L_0$). The abscissa gives the ratio $R = S_2^B/S_1^B$, a measure of surface energy symmetry. The phase fields are labeled with the abbreviations given in Figure 2a, designating the conditions for which each morphology is predicted to be stable. The gray strip along the FL/HL border delineates a metastable region of the HY morphology. Generally, the features in this example appear in all of the calculated phase diagrams except for the lowest $N$ ($N = 100$, 125) and highest $S_1^B$ ($-0.9\ kT$) cases, discussed later.

The rightmost section of Figure 2b shows the morphological behavior of the system in the limit of symmetric surface energetics ($R = 1$) and marks the overlap with previous theoretical treatments.[12,14,22,23,25,26] Here, at the point labeled **A**, a single morphological transition occurs from FL to PL, as other studies have predicted.[14,22,25,26] Moving toward the left, the perpendicular phase field splits, giving way to a region in which the HY structure gains stability. As the surface energetics become more asymmetric, another new phase field, the HL morphology, develops at point **C**. Thus, as the surface interactions become more asymmetric, morphologies that lack a horizontal plane of symmetry (i.e., HY and HL) are favored. On the whole, the system behavior can be divided into two distinct regimes based upon the existence of a stable HL phase and, accordingly, the $R$ coordinate of point **C**, denoted $R^*$ (Figure 2b). Below $R^*$, a stable HL phase intervenes in the transition from FL to the perpendicular structures (HY and PL), while above $R^*$, this transition is direct.

While FL, PL, and HL have been seen in other theoretical studies of copolymer thin film morphology, the HY structure has not been predicted previously and thus merits additional discussion. First, like the HL morphology, this structure is only stable when the surface energetics have some degree of asymmetry. Second, as seen in Figure 2b, the HY phase field is typically situated between the surface-parallel morphologies (FL and HL) and the PL phase. With both surface-parallel and surface-perpendicular elements, the HY structure may be seen as a "compromise" morphology that serves as an intermediate between fully parallel and fully perpendicular states. Moreover, the metastable existence of the HY morphology between the FL and HL phase fields suggests that such hybrids are possible intermediates between parallel symmetric and antisymmetric morphologies as well. This possibility will be pursued further in the discussion of our experimental results.

The effects of $N$, $\chi_{AB}$, and $S_1^B$ on the morphological behavior of this film system can be gauged, in part, by demonstrating how these variables affect the positions of coexistence curves in the calculated phase diagrams. Interestingly, the position of the FL to HL transition at $R = 0$ was found to be virtually constant, irrespective of $N$, $\chi_{AB}$, and $S_1^B$, with a value of $t = (0.7 \pm 0.01)L_0$. Figure 3 is provided to facilitate discussion of the molecular parameters. Figure 3A recapitulates the phase diagram in Figure 2b and provides a point of comparison by which the effect of each variable can be realized.

**Effect of $S_1^B$.** Comparing parts A and B of Figure 3 demonstrates the effect of the surface potential, $S_1^B$, on the behavior of the polymer film system. In Figure 3B, all system parameters are identical to those in Figure 3A, except $S_1^B$, which takes the value $-0.9\ kT$ ($S_1^B = -0.1\ kT$, inset). In comparing these figures, increasing the magnitude of $S_1^B$ is seen to stabilize those morphologies that exhibit a high degree of contact between the B-segments and the film surfaces. Hence, increasing $S_1^B$ favors the FL morphology while decreasing the size and extent ($R^*$ moves left) of the HL phase field. This stabilization of FL can also be seen at $R = 1$, where the FL to PL transition thickness decreases when the degree of B-segment surface attraction is increased, a trend established by previous studies.[14,22]

This inclination toward B segment−surface contact is also seen when tracking the effect of $S_1^B$ on the perpendicular morphologies, HY and PL. When $|S_1^B|$ is low (see Figure 3B, inset), the PL morphology is the only perpendicular structure expressed. Further, in this case, the gray strip in Figure 2b which denotes HY metastability becomes a region of PL stability, and the FL to PL transitions generally move to greater thicknesses. This emergence of PL is due to the decreased importance of B segment−surface contact on the system behavior. Upon increasing $|S_1^B|$ (Figure 3A), the PL phase gives way to the HY structure which has a higher degree of B surface contact, except when $R \approx 1$, where the PL phase always dominates. When the surface potential is very high (Figure 3B), PL is eliminated entirely, and the phase diagram collapses to two dominant phase fields (FL and HL) with a tiny intermediate HY region.

**Effect of $\chi_{AB}$.** The segmental interaction parameter, $\chi_{AB}$, determines the interfacial energy between A and B domains. Accordingly, increasing $\chi_{AB}$ favors those morphologies with comparatively small interfacial areas. The effects of segment−segment interaction can be seen by comparing parts A and D of Figure 3, wherein $\chi_{AB}$ is increased from 0.1 to 0.15. Immediately notable is the lack of HY structures at the higher $\chi_{AB}$. This is expected, given the large and curved A/B interface inherent in the HY morphology. Among the parallel morphologies, increasing $\chi_{AB}$ increases the stability of HL with respect to FL, which has twice the interfacial area (per unit volume). This accounts for the corre-

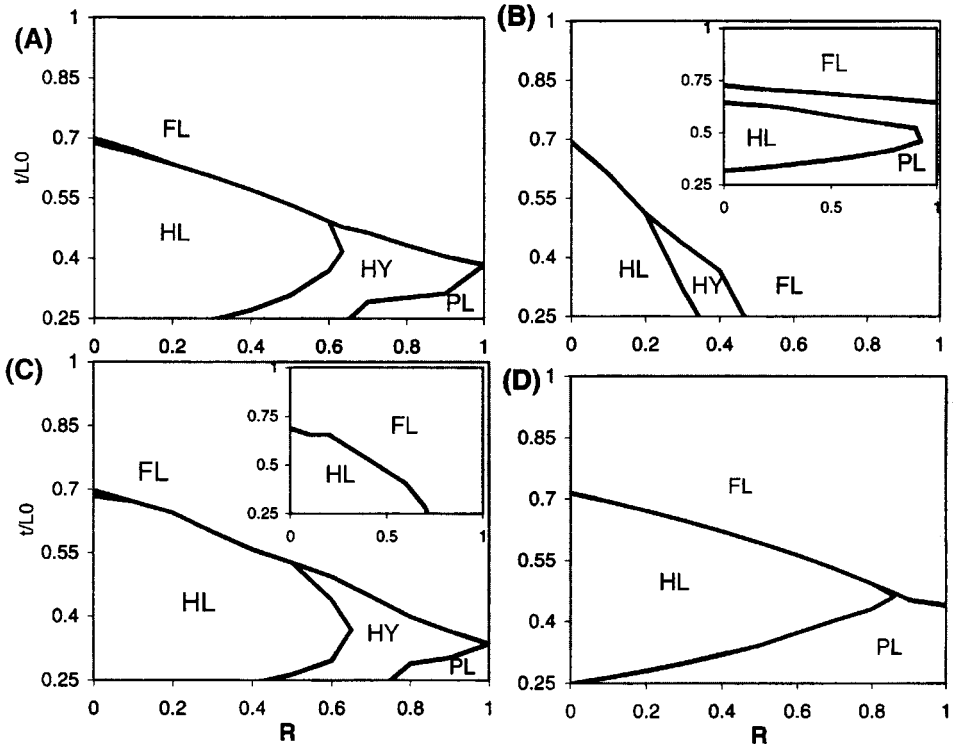


**Figure 3.** Phase diagrams illustrating the effect of the molecular parameters. (A) Recapitulation of Figure 2b for comparison. Each phase diagram (B), (C), and (D) changes the value of one variable from this case where $N = 200$, $S_1^B = -0.3\ kT$, and $\chi_{AB} = 0.1$, while keeping the remaining constant. (B) Effect of $S_1^B$: main plot, $S_1^B = -0.9\ kT$; inset, $S_1^B = -0.1\ kT$. (C) Effect of $N$: main plot, $N = 150$; inset, $N = 125$. (D) Effect of $\chi_{AB}$: $\chi_{AB} = 0.15$.

sponding shift in $R^*$ toward the right of the phase diagram when part A of Figure 3 is compared to part D.

The transition from FL or HL to PL is largely mediated by considerations of the interfacial energy, since for thicknesses below $L_0$, and then below $0.5L_0$, this perpendicular phase exhibits a lower interfacial area (assuming flat interfaces) than the respective surface-parallel state.[14] Thus, as $\chi_{AB}$ is increased, the stability of PL is enhanced with respect to the parallel morphologies. This shifts the HL/PL and FL/PL coexistence curves to higher values of $t/L_0$ as seen in Figure 3. Of course, as noted above, the PL A/B interfaces calculated in this study exhibit some degree of curvature due to the attraction of B segments to the surfaces.[55] This curvature, which increases with $S_1^B$, but decreases with $\chi_{AB}$, leads to generally lower transition thicknesses as compared to those predicted by assuming flat interfaces.[14]

**Effect of *N*.** The degree of polymerization, $N$, also affects the positions of the phase boundaries. There are, of course, shifts in absolute transition thickness—these have been normalized via the calculated $L_0$ for each molecular length. Beyond this obvious scaling relation, increasing $N$ tends to stabilize the perpendicular phases. Comparing parts A and C of Figure 3 demonstrates the effect of changing $N$ from 200 to 150 (125, inset) while keeping the remaining system parameters static. For our lowest $N$ systems (100, 125) perpendicular phases failed to appear at all. For these cases, a two field phase diagram was obtained as shown in Figure 3C (inset). Increasing $N > 150$ leads to a slight increase in both the size of the HY phase field and the thickness at which the HL/HY transition occurs, as can be seen by comparing parts A and C of Figure 3 (main). A similar inclination is seen for the FL/PL and FL/HY boundaries.

The effect of $N$ on the stability of the HY phase may be understood by considering the energetics of HY formation from the HL state. In part, the energetic advantage to HY formation is the expression of B segments at the $S_2$ surface, while the energetic barrier to forming these structures is the creation of the curved A/B interface. A simple analysis of the magnitude of these energetic terms (discussed in detail in ref 51) reveals that, for equivalent expression of B segments at $S_2$, the interfacial barrier is lower for larger $N$ systems as compared to smaller chain lengths. Accordingly, HY structures would be expected to first appear in progressively thicker films (relative to $L_0$) as $N$ is increased. This is the trend exhibited in the calculations and, as will be discussed below, observed in the experimental data.

**Experimental Observations.** When comparing our SCF calculations with experimental observations, an important difference between the two must be noted. While the SCF system is sandwiched between impenetrable boundaries, the experimental system has a single constrained surface. The consequence of this difference is quite apparent for substrate supported films thicker than $L_0$. Indeed, the formation of so-called "islands" and "holes" in films of an initial thickness that is incommensurate with a multiple of $L_0$ (or $(n + {}^1/_2)L_0$ for antisymmetric systems) can be directly attributed to this fact.[3,57] For these systems, the free surface is allowed to realize thicknesses that minimize the energy of the system.[22,57] Thus, as has been well-established experimentally, films of thickness $t > L_0$, where $nL_0 < t < (n + 1)L_0$, will, upon annealing, form a stepped surface with regions of two quantized thicknesses, $nL_0$ and $(n + 1)L_0$, the area proportions of which correspond to $1 + n - (t/L_0)$ and $(t/L_0) - n$, respectively.[3,5,57] The

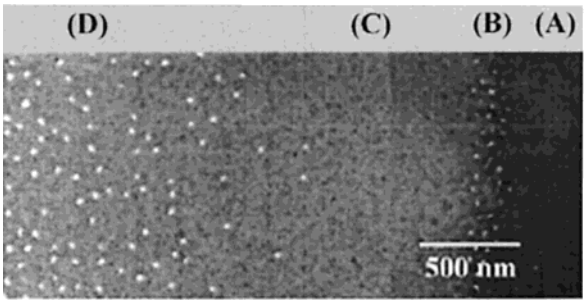


**Figure 4.** Plan view TEM micrograph showing section of PS-*b*-PBMA 250 DBC film which decreases in thickness from (A) to (D).

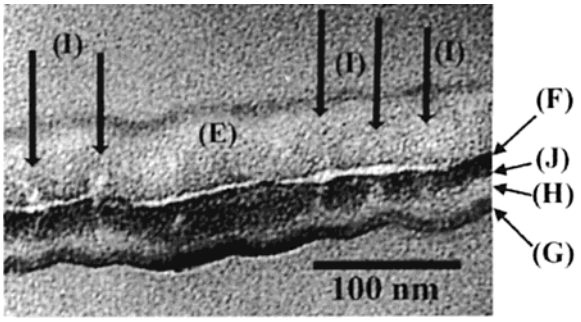


**Figure 5.** Cross-sectional TEM micrograph of PS-*b*-PBMA 250 DBC film showing a "hybrid" morphology (emphasized by vertical black arrows) comparable to that in Figure 4D.

current study finds that this trend continues in a similar manner for films with thickness below $L_0$. However, instead of $L_0$ jumps between thickness steps, these sub-$L_0$ systems make leaps of approximately $^1/_2L_0$, as will be discussed below.

**1. TEM Results**. The TEM micrograph in Figure 4 shows a plan view of a 250 K polystyrene-*b*-poly(butyl methacrylate) (PS-*b*-PBMA) thin film peeled from a silicon substrate. In this section of film, a thickness gradient exists such that at the rightmost portion of the micrograph the film is about $L_0$ thick (62.5 nm for this material) while the leftmost edge is somewhat below $0.5L_0$. This micrograph demonstrates the same thickness trends in morphological behavior exhibited by our SCF calculations (see, for example, Figure 2). The regions A and C have thicknesses of approximately $L_0$ and $0.5L_0$, respectively. The lack of contrast in these regions indicates surface-parallel morphologies. The full lamellar (FL) structure, observed at (A), exhibits half-layers of PBMA at the substrate and free surface. Region C shows the half-lamellar (HL) morphology, which presumably consists of a layer of PBMA at the substrate and a layer of PS at the free surface.

Points B and D show sections which are $t \approx 0.75L_0$ and $t < 0.5L_0$, respectively. The light features are the unstained PBMA domains oriented perpendicular to the film plane. The structures at (B) are "terrace edge" defects first studied by Carvalho and Thomas.[7] These structures form an intermediate state between the FL and HL morphologies and, while presumably stable, invite comparison with the metastable HY intermediate found between the calculated FL and HL phase fields in Figure 2b. Point D illustrates a "hybrid" morphology quite similar to the HY structure predicted by the SCF calculations. While the predicted and observed HY morphologies cannot be directly equated, due to the 2-dimensional nature of the SCF model, the latter appears to be the 3-dimensional analogue of the former, based upon several striking points of comparison. First and foremost, both the predicted and observed HY structures consist of contiguous surface-parallel and surface-perpendicular components of the same block species. Second, both exhibit an asymmetric distribution of block components at the top surface. One can immediately see these similarities by comparing Figure 2a (HY) with the TEM cross section shown in Figure 5, which illustrates a section of film in the thickness range of point D in Figure 4. The ribbon of film in this micrograph is tilted slightly with respect to the viewing plane. As a result, the free surface of the film can be seen at the top of the sample section (E). The two dark layers that sandwich the film (F and G) are the layers of carbon introduced during the sample preparation (peeling and microtomy). The light layer (H) shows the PBMA layer that originally resided at the substrate. Surface-perpendicular protrusions of PBMA (I) extend from this bottom layer through the darker PS layer (J) to the free surface, producing a profile very similar to that shown in Figure 2a (HY).

Returning to the micrograph shown in Figure 4, it can be seen that these surface-perpendicular PBMA domains have a cylindrical profile, appearing as light circles in this plan view. This is in contrast to the 2-dimensional calculated morphology which would, if imaged in plane view, show stripes of B monomer separated by domains of A, since spatial uniformity in the $y$ dimension is assumed in the model. While this difference illustrates the limitations of 2-D calculations, it should be noted (along with the arguments posed above) that the sizes of both the calculated and observed surface-perpendicular domains adhere to the dominant length scale of the copolymer system, being approximately $0.5L_0$ in width. Furthermore, both the calculated and observed morphologies appear in the same thickness range, i.e., $t < 0.5L_0$, positioned identically between the HL (or FL, depending on surface energetics) and PL structures. Note that the HL and HY structures are predicted stable only for asymmetric surface energetics.

**2. AFM Study of Copolymer Microdroplets**. Figure 6 shows an example of a dual height/phase AFM micrograph collected on a polystyrene-*b*-poly(lauryl methacrylate) (PS-*b*-PLMA) copolymer droplet edge. Using the height data (top), the film thickness of any section of the phase image can be determined. In the phase portion of Figure 6 (bottom), lighter regions are harder, while darker regions are softer. The very light band at the left of the image (labeled E) is the silicon substrate. The microdroplet of copolymer begins and increases in thickness as one moves toward the right of the micrograph. From the height data, the film thickness increases through two sharp steps, each roughly $0.5L_0$ in height. In the region labeled A, the film thickness was measured to be $L_0$ (54 nm). As indicated by the lack of contrast at this point, the surface-parallel FL morphology exists here. Note that, unlike the PS-*b*-PBMA sample shown in Figure 4, no surface-parallel HL morphology exists in this system. The direct thickness transition from FL to HY is seen at point B where the film is $0.43L_0$. Hereafter, the transition thickness at which surface-perpendicular domains are first expressed will be termed $t^*$. The dark circular domains represent softer PLMA domains expressed at the surface. These features are approximately $0.5L_0$ in width

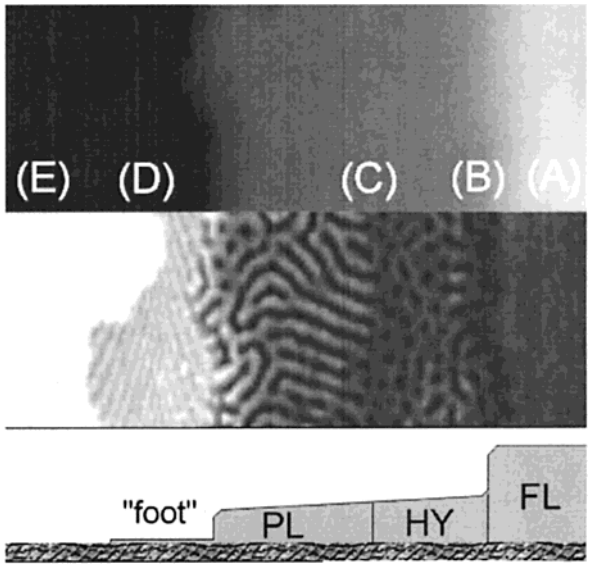


**Figure 6.** AFM height/phase micrograph of PS-*b*-PLMA 170 DBC droplet edge. The top portion of the micrograph is height data, and the bottom is phase data. Film thickness decreases toward the left of the micrograph where an area of bare substrate can be seen. Below the micrograph is a schematic cross section of the film labeled with morphology abbreviations.

**Table 3. Summary of Morphological Trends**

| diblock copolymer | FL | HL | HY | PL | notes |
|---|---|---|---|---|---|
| PS-*b*-PLMA 170 | yes | no | yes | yes | |
| PS-*b*-PLMA 50 | yes | no | yes | yes | |
| PS-*b*-PHMA | yes | no | yes | yes | |
| PS-*b*-PBMA 140 | yes | yes | yes | yes* | TEM |
| PS-*b*-PBMA 250 | yes | yes | yes | yes* | |
| PS-*b*-PBMA 650 | yes | yes** | yes | no | |
| PS-*b*-PPMA | yes | yes | yes | yes* | |
| PS-*b*-PEMA | yes | yes | yes | yes* | |
| PS-*b*-PMMA | yes** | yes | no | no** | ** [a] |

[a] See text.

with mean spacing just greater than $L_0$. A second transition (hereafter, $t^{**}$) from the HY to PL morphology is seen at point C, with $t^{**} \approx 0.3L_0$. Again, the pattern of thickness-dependent morphology reflects that illustrated by the SCF calculations, for example, at $R = 0.8$ of Figure 2b. In each case, the morphology starts with FL, bypasses the HL, and transforms directly into a HY structure, finally ending at the droplet edge with the PL morphology. This trend is illustrated in the schematic cross section found at the bottom of Figure 6.

In region D of Figure 6, a uniformly thick "foot" of material borders the very edge of the copolymer droplet. This feature is approximately 15 Å high and exhibits a lack of phase contrast.[58] This thin border was observed for all the DBC films studied. Similar features were noted by Henkee et al., who observed a halo of apparently unordered material around ordered copolymer droplets via TEM.[13] On the basis of the location and thickness of this region, it is hypothesized to be a "precursor" film analogous to the monomolecular films observed to precede homopolymer droplets spreading on smooth substrates.[59,60] A definitive determination of this fact and of the exact morphology of the proposed monolayer, however, requires further study.

Table 3 summarizes the qualitative thickness−morphology trends observed for the block copolymers in Table 2. These data show three distinct trends. In one copolymer, PS-*b*-PMMA, there was a complete lack

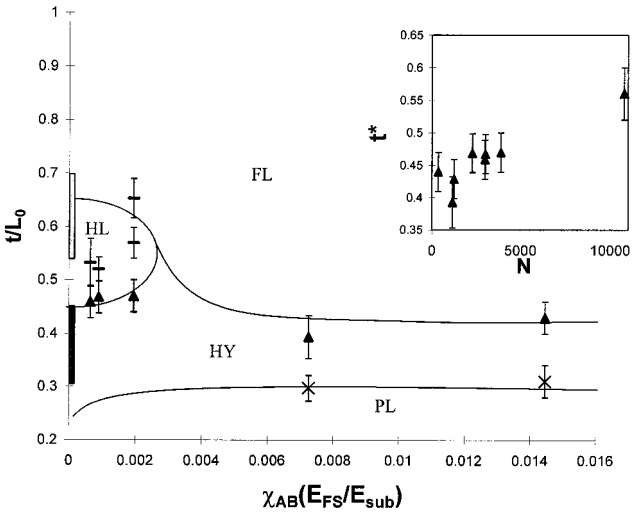


**Figure 7.** Summary of critical film thicknesses (relative to $L_0$) plotted as a function of the energetic parameter $\chi_{AB}(E_{FS}/E_{sub})$: FL/HL transitions (dashes), $t^*$ transitions (triangles), $t^{**}$ transitions (X's). The lines delineate the phase fields the data suggest. The dark gray bar on the left indicates the range of $t^*$ values predicted by the SCF calculations. The lighter gray bar indicates the predicted range for FL/HL. The block copolymer molecules are, in order from left to right: PS-*b*-PMMA, PS-*b*-PPMA, PS-*b*-PEMA, PS-*b*-PBMA 140, PS-*b*-PBMA 250, PS-*b*-PHMA, PS-*b*-PLMA 170. Inset: effect of the chain length, $N$, on the $t^*$ transition.

of lateral structure near $0.5L_0$. Only surface-parallel morphologies of thickness $0.5L_0$ and $^3/_2L_0$ were noted. (A more complete discussion of PS-*b*-PMMA can be found below.) PS-*b*-PEMA, PS-*b*-PPMA, and PS-*b*-PBMA show a second trend. In these materials FL, HL, HY, and PL morphologies were observed, with a sharp drop in thickness between the FL and HL states and a gradual thickness change from the onset of the HL morphology to $t^*$. A third sequence of morphologies was noted for the PS-*b*-PHMA and PS-*b*-PLMA systems. Here, only FL, HY, and PL morphologies were observed, with thickness changes following the pattern shown for PS-*b*-PLMA in Figure 6. The latter two morphological trends match those of the two regimes separated by $R^*$ in Figure 2b.

To better compare the experimental system to the calculations, Figure 7 plots thickness transitions as a function of $t/L_0$ and $\chi_{AB}(E_{FS}/E_{sub})$, calculated for each copolymer system from the values in Table 2. Here, $E_{FS}/E_{sub}$ is an approximation of $S_2^B/S_1^B$, while $\chi_{AB}$ accounts for the variation of this parameter in the experimental data. The variation of $N$ ($L_0$) among the copolymers was minimized by plotting data only from copolymers with $L_0$ values within one standard deviation of the mean $L_0$ value ($L_0 = 53.4 \pm 27$ nm). Shown on the graph are the FL/HL (dashes), $t^*$ (triangles), and $t^{**}$ (Xs) thickness transitions as measured (if they exist) for each block copolymer system. Plotted in this manner, the data suggest the phase fields roughly defined by the solid lines. In several respects, this experimental morphology map mirrors the phase diagrams generated from the SCF calculations, for example, Figure 2b. For the most asymmetric systems two transitions are seen, from FL to HL and from HL to HY ($t^*$), the former at thickness values above $0.5L_0$ and the latter below $0.5L_0$. While the FL/HL transitions fall well within the range of values predicted by the calculations (light gray bar), measured $t^*$ values are higher than the calculated values (dark gray bar), suggesting that the calculations

underestimate the stability of the HY phase. This discrepancy may be due to the fact that the chain lengths used in the calculations are much shorter (due to computational constraints) than those in the experimental systems. As discussed above, the calculations predict a stabilization of the HY morphology as $N$ increases. Further, as discussed below, this $N$ dependence is also reflected in the experimental observations.

Moving to the right in Figure 7, a direct transition from FL to HY ($t^*$) is observed followed by the $t^{**}$ transition from HY to PL. In this more symmetric regime, both the $t^*$ and $t^{**}$ transitions fell within the ranges predicted by the calculations, as can be seen by comparing these values with the phase diagrams shown in Figure 3.

The inset of Figure 7 plots the molecular weight dependence of the $t^*$ transitions measured for the entire body of DBCs in the experimental study. The number of statistical segments per chain is calculated using values from Table 2, assuming the relation[61]

$$L_0 = 2\left(\frac{1}{3}\sqrt{\frac{\chi_{AB}}{6}}\right)^{1/3} N^{2/3} a$$

Here, $a$ is taken as the average value of the statistical segment length between the methacrylate (Table 2) and polystyrene (6.7 Å). The data show a modest but notable increase in $t^*$ as $N$ increases. This trend suggests the enhanced stability of perpendicular morphologies with increasing $N$, as predicted by the SCF calculations, which may account for differences between the predicted and observed $t^*$ values.

**3. Relation to Antisymmetric Surface Interactions**. Thin films of polystyrene-*b*-poly(methyl methacrylate) (PS-*b*-PMMA) on silicon exhibit a behavior different than that of the rest of the PS-*b*-poly(*n*-alkyl methacrylate) copolymer family. While PMMA (similar to the other *n*-alkyl methacrylates) has a favorable interaction with the native silicon oxide, the surface tension of PS is comparatively lower. Thus, this system favors *antisymmetric* morphologies that have PS at the free surface and PMMA at the substrate.[6] Accordingly, the first two stable parallel morphologies of PS-*b*-PMMA are HL (PS up, PMMA adjacent to the substrate, near $0.5L_0$) and a $^3/_2$ FL lamellar structure at $^3/_2L_0$, illustrated schematically in Figure 8B.

The PS-*b*-PMMA system has been studied extensively by various research teams.[3,6,33−35,62] While most of the data collected through these studies are well understood, at least two groups have reported a surface-perpendicular morphology for films of PS-*b*-PMMA on silicon for thicknesses near $L_0$. This seems inconsistent with many observations (including those above), since a commensurate $L_0$ film thickness would be expected to generate a surface-perpendicular phase, e.g. FL. This "unconventional morphology" was first noted by Russell et al.,[6] who showed using neutron reflectivity and X-ray photoelectron spectroscopy that the $L_0$-thick films had PMMA at the substrate, an inner layer of PS, and a layer of mixed PS and PMMA at the free surface. Later, Morkved and co-workers used TEM and AFM to demonstrate that PS-*b*-PMMA films near $L_0$ in thickness display a laterally organized surface structure[33,34] and proposed a morphology[33] consistent with these results, illustrated in Figure 8A. Matsen, using SCF calculations, predicted a similar structure between symmetric boundaries provided the copolymer composition was somewhat asymmetric,[22] while Tang and Witten accomplished this by imposing boundary conditions that "quenched" the bottom (substrate) half of the structure into a static HL morphology.[24]

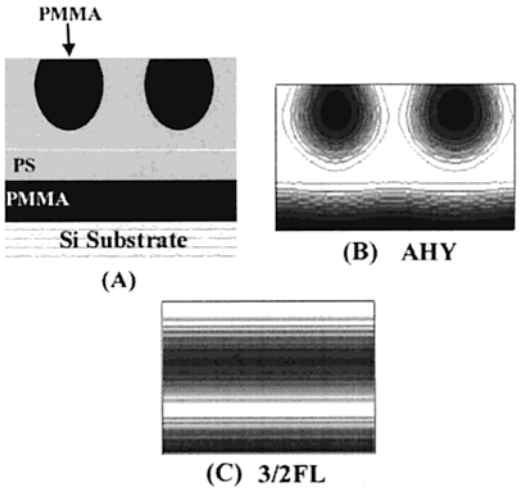


**Figure 8.** Summary of antisymmetric morphologies and their abbreviations. (A) Schematic of lateral morphology proposed for PS-*b*-PMMA DBC film systems.[24,33] (B) Antisymmetric hybrid morphology predicted by the SCF calculations. (C) Antisymmetric $^3/_2$ FL morphology.

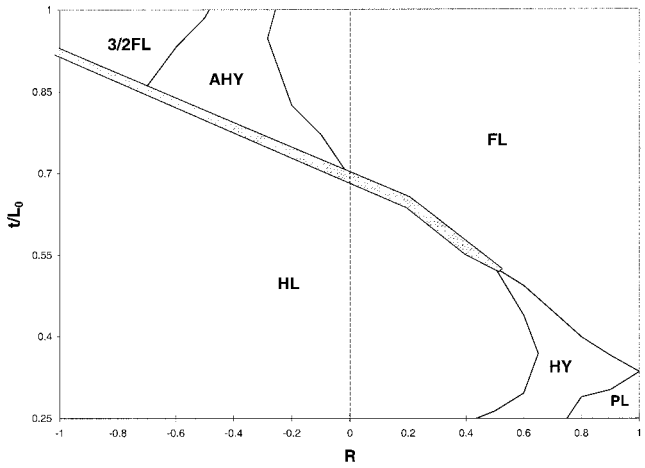


**Figure 9.** Complete (symmetric + antisymmetric) phase diagram for $N = 150$, $S_1^B = -0.3\ kT$, and $\chi_{AB} = 0.1$. Phase fields are labeled with abbreviations from Figure 8. The gray area delineates where the HY structure is metastable.

To further understand this popularly studied system, we extended our calculations to include surface energetics that model PS-*b*-PMMA on silicon, in which case the surface energetics are both *antisymmetric*, i.e., $S_1$ favors B segments, $S_2$ favors A segments, and *asymmetric*, meaning the magnitude of $S_1^B$ and $S_2^A$ are different. Accordingly, for this system, $R$ is negative, like the $E_{FS}/E_{sub}$ value for PS-*b*-PMMA shown in Table 2. With $N = 150$, $S_1^B = -0.3\ kT$, and $\chi_{AB} = 0.1$, it is the conjugate system to that shown in Figure 2c. Figure 8 summarizes the morphologies generated by the antisymmetric boundary conditions, and Figure 9 shows these structures in the context of a complete phase diagram that spans the full range of $R$ from −1 to 1. The antisymmetric hybrid morphology (Figure 8B, hereafter, AHY), identical to that proposed by Morkved and co-workers,[33] inhabits a phase field located in the $t \sim L_0$ regime, bounded by FL, HL, and $^3/_2$ FL domains.

The AHY may be seen as a fusion of two half-period films, each with local asymmetric surface energetics. The HL morphology, constituting the bottom half of the film, optimizes $S_1^B$ energetics, since the PMMA (B) block wets the substrate. (This was implicit in the calculations of Tang and Witten.[24]) In the top half of the film, the A segments (PS) are favored at both the free surface *and* the HL "substrate", but with differing affinities, now determined by the differential surface energies and the attraction of A for itself. The consequence is the formation of the *hybrid morphology*, where A segments (PS) now form the contiguous surface-perpendicular features. Hence, the HL and HY structure combine to form the AHY morphology.

## Concluding Remarks

This deconstruction of the AHY structure is interesting in ways that transcend the particulars of the PS-*b*-PMMA film system. When considered in this light, the behavior of PS-*b*-PMMA is identical to the other PS-*b*-(*n*-alkyl methacrylates), only shifted $0.5L_0$ in thickness and with an appropriate phase inversion to accommodate local boundary conditions. The latter exhibits the HY morphology near $0.5L_0$, while the former exhibits the HL structure combined with an inverted HY component near $L_0$. A conjugate trend is already known to govern the sequence of stable surface-parallel states in each case;[2−5] i.e., symmetric systems exhibit a surface-perpendicular state at $L_0$, while antisymmetric systems find these at $0.5L_0$ and $^3/_2L_0$. Thus, sub-$L_0$ thick films are unified under the "$nL_0$ and $(n + {}^1/_2L_0)$" paradigm widely used to describe the morphology of thicker films.[3−5] Framing the question in this manner also suggests that the structure of thin lamellar films can be understood through a general "half-period" principle of morphological development. It seems that the film morphology *in any thickness regime* can be deduced by considering the relative strength of the surface energetics imposed on the half-period components of the film. Thus, for example, at $L_0$, symmetric systems form the FL structure consisting of two stacked HL structures, one phase inverted with respect to the other, each arranged such as to optimize the surface and interfacial energetics. In contrast, antisymmetric systems of the same thickness may form the AHY, composed of an HL plus an overlying HY structure that represents the phase inverted form of the HY structure seen in symmetric systems at $0.5L_0$. Indeed, as this "half-period" principle seems to apply to the structure of thicker lamellar films also, it may well be a way of reexamining lateral morphologies seen for noninteger (or half-integer) thicknesses, like the terraced-edge defects[7] discussed above. Generally, these concepts also represent a conceptual framework for examining the morphologies of more complex DBC systems. Recent studies of thin film morphology in DBC systems containing a liquid-crystalline component, for example, have benefited from such analysis.[63] Further, Kim and Russell[64] have recently observed hybrid morphologies in cylinder-forming DBC systems. It will be interesting to see whether the principles outlined here can be extended to such compositionally asymmetric copolymers as more information about these film systems becomes available.

**Acknowledgment.** M.J.F. and A.M.M. thank E. L. Thomas and E. L. Shaw for helpful conversations. This work was supported primarily by the MRSEC Program of the National Science Foundation under Award DMR 98-08941. A.C.B. thanks the National Science Foundation for financial support under Grant 9709101.

## References and Notes

(1) Bates, F. S.; Fredrickson, G. H. *Annu. Rev. Phys. Chem.* **1990**, *41*, 525.
(2) Matsen, M. W. *Curr. Opin. Colloid Interface Sci.* **1998**, *3*, 40.
(3) Russell, T. P.; Coulon, G.; Deline, V. R.; Miller, D. C. *Macromolecules* **1989**, *22*, 4600.
(4) Anastasiadis, S. H.; Russell, T. P.; Satija, S. K.; Majkrzak, C. F. *Phys. Rev. Lett.* **1989**, *62*, 1852.
(5) Ausserre, D.; Chatenay, D.; Coulon, G.; Collin, B. *J. Phys. (Paris)* **1990**, *51*, 2571.
(6) Russell, T. P.; Menelle, A.; Anastasiadis, S. H.; Satija, S. K.; Majkrzak, C. F. *Macromolecules* **1991**, *24*, 6263.
(7) Carvalho, B. L.; Thomas, E. L. *Phys. Rev. Lett.* **1994**, *73*, 3321.
(8) Fredrickson, G. H. *Macromolecules* **1987**, *20*, 2535.
(9) Turner, M. S. *Phys. Rev. Lett.* **1992**, *69*, 1788.
(10) Shull, K. R. *Macromolecules* **1992**, *25*, 2122.
(11) Kikuchi, M.; Binder, K. *Europhys. Lett.* **1993**, *21*, 427.
(12) Kikuchi, M.; Binder, K. *J. Chem. Phys.* **1994**, *101*, 3367.
(13) Henkee, C. S.; Thomas, E. L.; Fetters, L. J. *J. Mater. Sci.* **1988**, *23*, 1685.
(14) Walton, D. G.; Kellogg, G. J.; Mayes, A. M.; Lambooy, P.; Russell, T. P. *Macromolecules* **1994**, *27*, 6225.
(15) Vandijk, M. A.; Vandenborg, R. *Macromolecules* **1995**, *28*, 6773.
(16) Kellogg, G. J.; Walton, D. G.; Mayes, A. M.; Lambooy, P.; Russell, T. P.; Gallagher, P. D.; Satija, S. K. *Phys. Rev. Lett.* **1996**, *76*, 2503.
(17) Mansky, P.; Chaikin, P. M.; Thomas, E. L. *J. Mater. Sci.* **1995**, *30*, 1987.
(18) Mansky, P.; Harrison, C. K.; Chaikin, P. M.; Register, R. A.; Yao, N. *Appl. Phys. Lett.* **1996**, *68*, 2586.
(19) Fasolka, M. J.; Harris, D. J.; Mayes, A. M.; Yoon, M.; Mochrie, S. G. J. *Phys. Rev. Lett.* **1997**, *79*, 3018.
(20) Huang, E.; Rockford, L.; Russell, T. P.; Hawker, C. J. *Nature* **1998**, *395*, 757.
(21) Park, M.; Harrison, C.; Chaikin, P. M.; Register, R. A.; Adamson, D. H. *Science* **1997**, *276*, 1401.
(22) Matsen, M. W. *J. Chem. Phys.* **1997**, *106*, 7781.
(23) Pickett, G. T.; Balazs, A. C. *Macromolecules* **1997**, *30*, 3097.
(24) Tang, W. H.; Witten, T. A. *Macromolecules* **1998**, *31*, 3130.
(25) Geisinger, T.; Muller, M.; Binder, K. *J. Chem. Phys.* **1999**, *111*, 5241.
(26) Geisinger, T.; Muller, M.; Binder, K. *J. Chem. Phys.* **1999**, *111*, 5251.
(27) Suh, K. Y.; Kim, Y. S.; Lee, H. H. *J. Chem. Phys.* **1998**, *108*, 1253.
(28) Radzilowski, L. H.; Carvalho, B. L.; Thomas, E. L. *J. Polym. Sci., Part B: Polym. Phys.* **1996**, *34*, 3081.
(29) Lambooy, P.; Russell, T. P.; Kellogg, G. J.; Mayes, A. M.; Gallagher, P. D.; Satija, S. K. *Phys. Rev. Lett.* **1994**, *76*, 2899.
(30) Koneripalli, N.; Singh, N.; Levicky, R.; Bates, F. S.; Gallagher, P. D.; Satija, S. K. *Macromolecules* **1995**, *28*, 2897.
(31) Koneripalli, N.; Levicky, R.; Bates, F. S.; Ankner, J.; Kaiser, H.; Satija, S. K. *Langmuir* **1996**, *12*, 6681.
(32) Giessler, K. H.; Rauch, F.; Stamm, M. *Europhys. Lett.* **1994**, *27*, 605.
(33) Morkved, T. L.; Jaeger, H. M. *Europhys. Lett.* **1997**, *40*, 643.
(34) Morkved, T. L.; Lopes, W. A.; Hahm, J.; Sibener, S. J.; Jaeger, H. M. *Polymer* **1998**, *39*, 3871.
(35) Huang, E.; Russell, T. P.; Harrison, C.; Chaikin, P. M.; Register, R. A.; Hawker, C. J.; Mays, J. *Macromolecules* **1998**, *31*, 7641.
(36) Stocker, W. *Macromolecules* **1998**, *31*, 5536.
(37) Vignaud, G.; Gibaud, A.; Grubel, G.; Joly, S.; Ausserre, D.; Legrand, J. F.; Gallot, Y. *Physica B* **1998**, *248*, 250.
(38) Harrison, C.; Park, M.; Chaikin, P. M.; Register, R. A.; Adamson, D. H.; Yao, N. *Polymer* **1998**, *39*, 2733.
(39) Radzilowski et al. (ref 28), for example, showed that for $t \ll L_0$ free-standing films of diblock copolymers which display ordered spheres in the bulk formed volume-asymmetric lamella.
(40) Spatz, J. P.; Sheiko, S.; Moller, M. *Adv. Mater.* **1996**, *8*, 513.
(41) Scheutjens, J. M. H. M.; Fleer, G. J. *J. Phys. Chem.* **1979**, *83*, 1619.
(42) This convention of interactions was chosen simply as a means of limiting the extensive variable space inherent to this system.

(43) Ruzette, A. V. G.; Banerjee, P.; Mayes, A. M.; Pollard, M.; Russell, T. P.; Jerome, R.; Slawecki, T.; Hjelm, R.; Thiyagarajan, P. *Macromolecules* **1998**, *31*, 8509.
(44) *Handbook of Semiconductor Wafer Cleaning Technology: Science, Technology and Applications*; Kern, W., Ed.; Noyes Publications: Park Ridge, NJ, 1993; p 436.
(45) Billmeyer, F. W. *Textbook of Polymer Science*; John Wiley & Sons: New York, 1962.
(46) Russell, T. P.; Hjelm, R. P.; Seeger, P. A. *Macromolecules* **1990**, *23*, 890.
(47) Ruzette, A.-V. G. Personal communication.
(48) Kämpf, G.; Hoffman, M.; Krömer *Ber. Bunsen-Ges. Phys. Chem.* **1970**, *71*, 851.
(49) Geil, P. H. *Polymer Single Crystals*; R. B. Krieger: Huntington, NY, 1973.
(50) Bassett, D. C. *Philos. Mag.* **1961**, *6*, 1053.
(51) Fasolka, M. J. Doctoral Thesis, Department of Materials Science and Engineering, Massachusetts Institute of Technology, 2000.
(52) Magonov, S. N.; Cleveland, J.; Elings, V.; Denley, D.; Whangbo, M. H. *Surf. Sci.* **1997**, *389*, 201.
(53) Magonov, S. N.; Elings, V.; Whangbo, M. H. *Surf. Sci.* **1997**, *375*, L385.
(54) Haugstad, G.; Jones, R. R. *Ultramicroscopy* **1999**, *76*, 77.
(55) Pickett, G. T. *J. Chem. Phys.* **1996**, *104*, 1657.
(56) Pereira, G. G.; Williams, D. R. M. *Macromolecules* **1999**, *32*, 1661.
(57) Coulon, G.; Collin, B.; Ausserre, D.; Chatenay, D.; Russell, T. P. *J. Phys. (Paris)* **1990**, *51*, 2801.
(58) The rippled look to parts of this region are due to a tapping mode AFM oscillation artifact.
(59) Ausserre, D.; Picard, A. M.; Leger, L. *Phys. Rev. Lett.* **1986**, *57*, 2671.
(60) Leger, L.; Erman, M.; Guinetpicard, A. M.; Ausserre, D.; Strazielle, C. *Phys. Rev. Lett.* **1988**, *60*, 2390.
(61) Ohta, T.; Kawasaki, K. *Macromolecules* **1986**, *19*, 2621.
(62) Russell, T. P.; Menelle, A.; Anastasiadis, S. H.; Satija, S. K.; Majkrzak, C. F. *Makromol. Chem., Macromol. Symp.* **1992**, *62*, 157.
(63) Wu, J. S.; Fasolka, M. J.; Hammond, P. T. *Macromolecules* **2000**, *33*, 1108.
(64) Kim, H. C.; Russell, T. P. Personal communication.
(65) Kirste, R. G.; Kratky, O. *Z. Phy. Chem. (Munich)* **1962**, *31*, 383.

MA990021H